Creation and Value of Synthetic High-Frequency Solar Simulations for Distribution System QSTS Simulations

Matthew Lave, Matthew J. Reno, Robert J. Broderick
Sandia National Laboratories, Livermore, CA and Albuquerque, NM, 94550 and 87185, USA

***Abstract* — Methods and initial results are presented for creating synthetic high-frequency solar simulations with unique profiles for each interconnection point on a distribution system feeder using low-frequency input data. The three steps to synthetic sample creation are to develop a relationship between high and low frequency data, create high-frequency timeseries based on this relationship, and then to generate unique samples for different spatial locations. The simulation results for a distribution system voltage regulator demonstrate the value of unique high-frequency samples for distributed PV compared to a single PV profile used at all interconnection points.**

I. Introduction

High-frequency solar variability datasets with unique inputs for different interconnection points on distribution feeders are important inputs to accurate quasi-static time series (QSTS) distribution grid integration studies [1]. Using low-frequency solar variability underestimates the impact of solar photovoltaics (PV) to distribution grid operations [2], while using a single PV profile for all interconnection points results in an overestimation of the PV impact due to the spatial smoothing provided by distributed PV [3].

Measurements of high-frequency solar variability are scarce, motivating methods which can synthetically generate high-frequency data from more ubiquitous low-frequency data such as satellite-derived irradiance [4]. In this paper, we present initial results from ongoing work to develop high frequency, spatially-unique synthetic samples and to show their value to QSTS.

II. Method

To create inputs to distribution grid studies which involve distributed PV across a feeder, Sandia will use a 3-step process.

1) Develop a relationship between low-frequency satellite derived solar irradiance and high-frequency solar irradiance, using an hourly or daily summary statistic such as the variability score (VS).
2) Select high frequency timeseries samples given the predicted high-frequency summary statistic.
3) Generate unique irradiance samples for each interconnection point by adding some decorrelation between points, while still retaining the overall summary statistics.

A. Low-frequency data and high-frequency data relationship

The relationship between low-frequency satellite and high-frequency irradiance has been established in previous work [5]. The relation between solar variability derived from hourly satellite irradiance versus sub-minute ground measured solar irradiance was found to be strongest when the hourly satellite data was adjusted in several ways.

The adjusted satellite data was first converted to a clear-sky index to remove solar variability caused by the sun's movement through the sky. Then, the median of all daily variability scores, using a year or more of satellite data, was used. This median variability score was then scaled by the ratio of $\frac{\text{median GHI}}{1000\,\text{Wm}^{-2}}$, to reintroduce the magnitude of irradiance that was removed by using the clear-sky index. Finally, spatial smoothing was used by taking the distance-weighted average of the 9 satellite pixels surrounding the location of interest. The ground 30-second variability is shown as a function of the 1-hour satellite variability in Figure 1, where the 1-hour satellite data was adjusted as described in the bullets above.

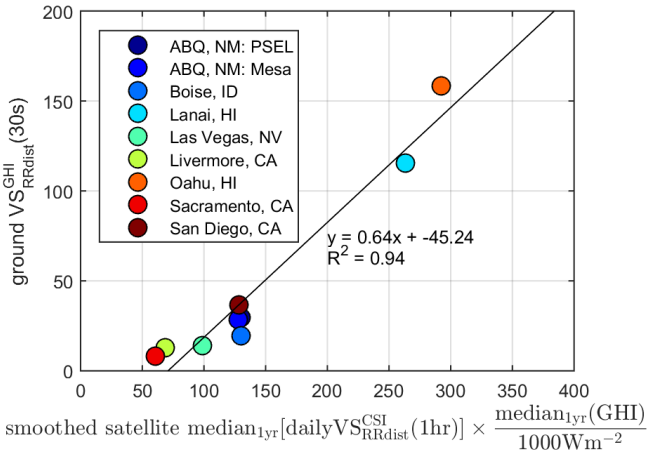

Figure 1: Relationship between 30-second ground measured solar variability (y-axis) and 1-hour satellite derived solar variability (x-axis) for several locations. [5]

B. Select High-Frequency Timeseries

At least three basic methods exist for selecting appropriate high-frequency timeseries based on the low-frequency variability determined in Section II. A.

One method is to find hours in a lookup library that match the summary statistic found from satellite data. For this method, a large database of high-frequency irradiance samples is needed. Based on the variability statistic assigned to each hour of satellite data, a representatively variable hour of high-frequency data is pulled from the library. Figure 2 shows an example of this method. Hours in the morning are clear and hence low-variability sample hours are assigned from the library. In the afternoon and evening, however, the hourly data indicates a sharp change in output, leading to a high variability

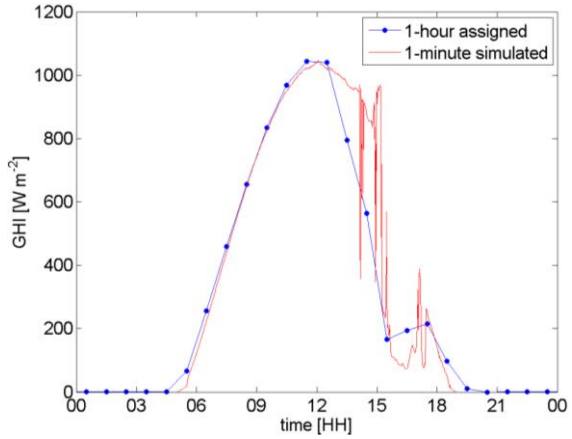

Figure 2: Example of using a library lookup to assign 1-minute high resolution data based on hourly variability statistic data.

statistic for those hours, and hence the high-frequency samples assigned from the library are highly variable. This method is similar to the one in [6] that was shown to work well, but it requires nearby high-resolution irradiance measurements and correlations with satellite data.

A second method is to create synthetic ramp rates by sampling from a cumulative distribution of high-frequency ramp rates for times which match the low-variability statistic. This method is similar to the first method, except that each short-interval ramp (e.g., 1-second or 1-minute) is sampled independently; in the first method, hour-long blocks are sampled all altogether. The advantage of this method is that it requires a smaller library of high-frequency data. The disadvantage is that, due to the independent sampling, special care must be taken to ensure that the autocorrelation of the created timeseries is representative of actual solar timeseries. That is, the independent sampling may, for example, often choose several large down ramps in a row, leading to a very steep decline in generation that is not reflected in the hourly data. Instead, additional dependencies must be factored into this method, such as that solar timeseries are more likely to ramp up after a down ramp than down again.

The third method, which we describe in detail in this paper, is the creation of synthetic cloud fields based on the hourly irradiance statistic. The cloud sizes are scaled based on the variability determined from the hourly data. Cloud fields are created based on a modification of Perlin noise [7], which has historically been used for creation of clouds for movies and video games. Just as for the second method, special care must be taken to accurately reproduce the ramp rate statistics of true solar irradiance timeseries. as this method tends to predict too quick of changes from full output to cloud obstruction. Smoothing of the cloud edges and retention of high-spatial scale (in addition to larger cloud features) noise are imperative.

C. Unique PV Production Across a Distribution Feeder

A single representative timeseries for all locations on a feeder will lead to significant overestimation of the PV impacts to the feeder (see Section IV), as all distributed PV systems will ramp at the exact same time and in the same direction. Instead, unique PV profiles must be created for each of the different interconnection points along the feeder to model cloud shading, movement, and the spatial smoothing of distributed PV.

The method utilized to create unique PV profiles will depend on the method to create representative timeseries. The first and second representative timeseries methods described in Section II. B. result in a single timeseries. These can then be tuned into unique timeseries by time-shifting each timeseries based on the cloud speed. Example time shifts for PV interconnection locations on a distribution feeder and an example shifted timeseries are shown in Figure 3. Time shifts must occur for clear-sky index data, as seen in Figure 3, to account for changing sun angles (most important over long time periods of 10s of minutes to hours), in addition to the cloud motion. The disadvantage to this method is that all locations perpendicular to the direction of cloud motion have identical PV generation timeseries, and all locations have identical irradiance statistics, just with different offsets. The results is that spatial smoothing

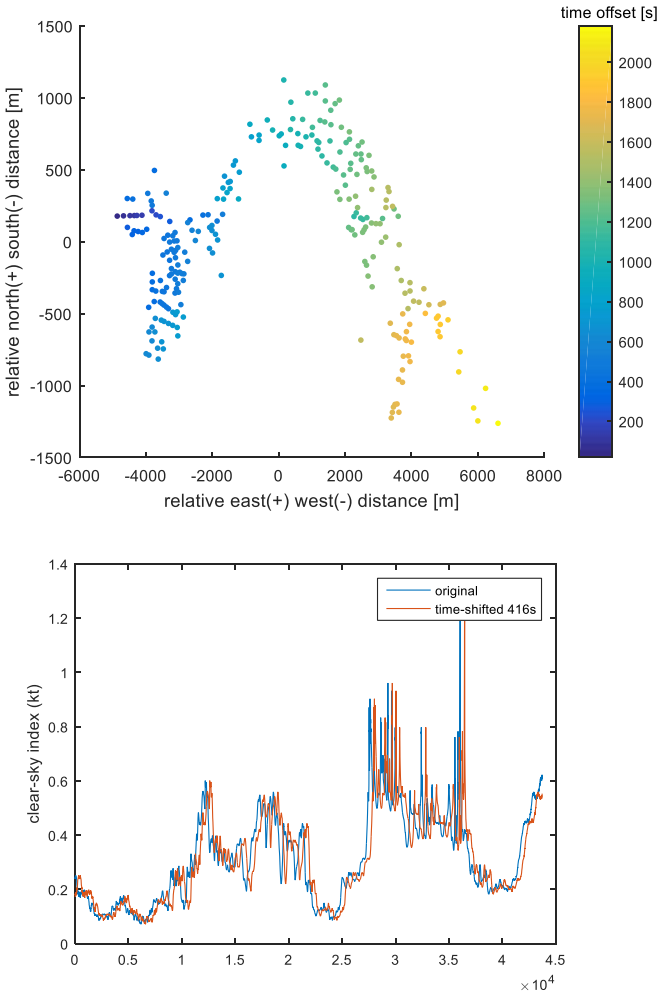

Figure 3: [Top] Time offset for points along a distribution feeder, and [Bottom] resulting shifted timeseries for one offset.

across the feeder is slightly underestimated, and, hence, the PV impact to the feeder may be slightly overestimated.

III. Synthetic Cloud Fields

For the synthetic cloud field method, the unique PV output profiles are naturally created due to the 2-dimentional nature of the cloud fields, Since the synthetic cloud fields have the ability to create high-frequency timeseries and unique PV production across a distribution feeder, it is a promising method. In this section, we present work we have done to develop the cloud field method and create unique high-resolution PV timeseries.

A. Field at Different Scales

The synthetic cloud fields method begins by creating random noise at different spatial scales, as seen in the left plots in Figure 4.

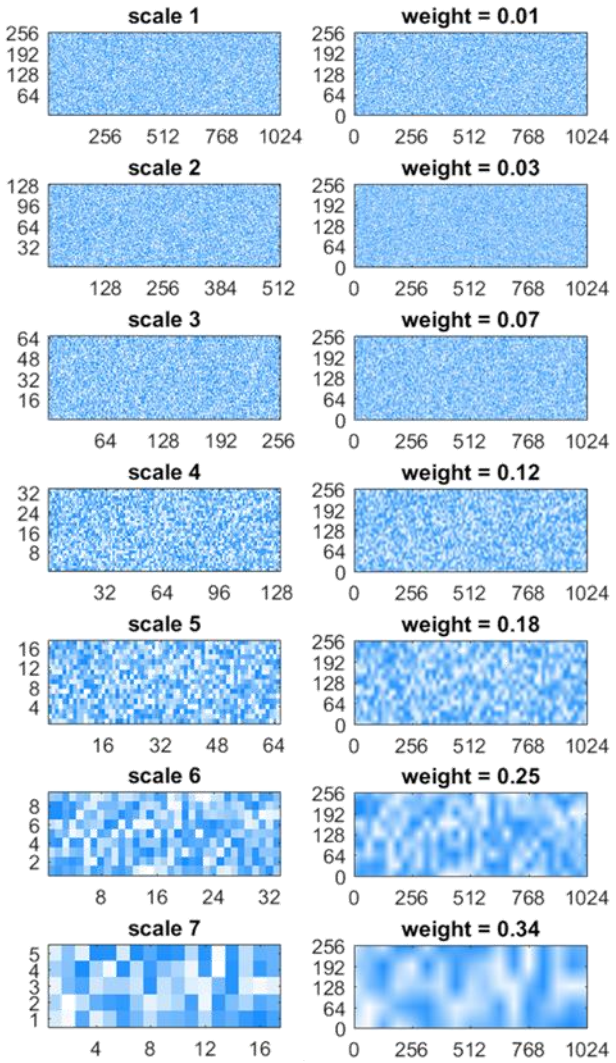

Figure 4: [Left] Finer to coarser (top to bottom) scales of random noise. [Right] Those random noise fields interpolated to the size of the finest random noise field (scale 1).

Next, each scale of random noise is linearly interpolated to a grid the same size as the finest grid (scale 1 in Figure 4). This results in a smooth field for the larger scales while retaining the more random field at the smaller scales, as seen in the right side of Figure 4.

B. Initial Cloud Field

These interpolated fields are added together to create an initial cloud field, as seen Figure 5. Different weights are applied to the different interpolated fields. These weights are related to the solar variability: a higher weighting on the finer interpolated fields will lead to higher variability since the resulting cloud field will be more jagged.

Here, we define scale weighting based on the variability score [8]. Specifically, weights are related to $i^{1/-\ln(VS)}$, where i is the scale and VS is the variability score. Research is on-going to determine the exact coefficients.

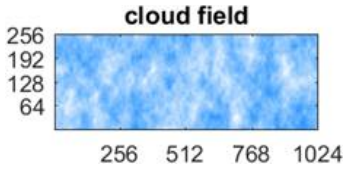

Figure 5: Initial cloud field created by summing all the interpolated fields (right plots in Figure 4).

C. Cloud Mask

However, this initial cloud field does not look like actual sky conditions: values range from fully clear to fully cloudy without distinct cloud shapes. To obtain more distinct clouds, we create a cloud mask, which is based on the expected fraction of the sky covered by clouds (e.g., as found from hourly data).

The cloud mask is created by setting all values greater than kt to clear sky. For example, if kt=0.5, then roughly half the pixels in the cloud field will be set to clear sky. Figure 6 shows an example cloud mask for kt=0.5, and the resulting cloud field when the mask is applied.

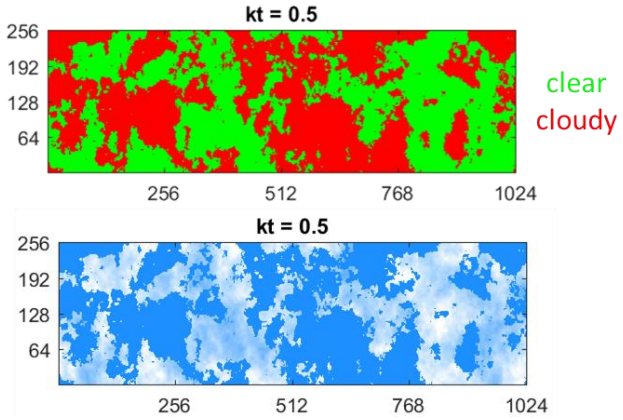

Figure 6: [Top] Cloud mask. [Bottom] Resulting cloud field after mask is applied.

To apply the cloud mask, two initial cloud fields are created. The first one is used to make the cloud mask, and the cloud mask is then applied to the second cloud field. If the cloud mask were applied to the same field as it was created from, there would be no values in the cloud field between kt and 1 (clear). This is especially a problem for low kt values, where, e.g., for kt=0.2, the clouds would all be very opaque (no values would be generated between 0.2 and 1).

D. Variation with VS and kt

We have defined the cloud fields to be a function of VS and kt. Figure 7 shows example cloud fields for a variety of VS and kt combinations. As VS increases, indicating more variability, the clouds get smaller. As kt increases, indicating less of the sky is covered by clouds, we see more clear sky.

Also included in Figure 7 is a clear-sky index sample. This was generated by sampling a complete row from each cloud field. Since the cloud fields have values ranging from 0-1, they are analogous to clear-sky index values: 0 is fully cloudy and 1 is fully clear.

These clear-sky samples again confirm that cloud fields with higher VS have higher variability, and that cloud fields with higher kt values tend to have fewer clouds. However, the clear-sky index samples in Figure 7 are not fully realistic. They tend to be either 1 (clear) or a value much less than 1 (cloudy), instead of having smooth transitions from clear to cloudy. Additionally, cloudy areas are highly opaque, which is not representative of thin clouds which only slightly reduce the irradiance reaching the surface.

We continue to modify the cloud field creation methodology, including adjusting the scale weights, applying targeted smoothing, and allowing for different cloud types and opacities [9]. The goal is to be able to match the statistics of ground measured irradiance.

E. Sampling from Cloud Fields

Since the eventual goal of the cloud field methodology is to create unique PV samples for distribution grid studies, we need to be able to sample timeseries from the cloud fields. We do this by assigning a length scale to the cloud field (e.g., one pixel is one meter), and by advecting the clouds based on the cloud speed. For example, for a 5 m/s cloud speed with 1m pixels, we would sample every 5 pixels to generate a 1-second resolution timeseries.

Examples of samples at various cloud speeds are shown in Figure 8. Fast clouds speeds lead to lower correlation among different PV sites [10], and we see this behavior in the samples from the cloud fields.

However, a side effect of sampling at different intervals is that the cloud speed is directly impacting the variability of each individual location: slower cloud speeds lead to less variability. The variability at each individual location should depend only on the VS (not the cloud speed), so this interdependency will need to be addressed in future iterations.

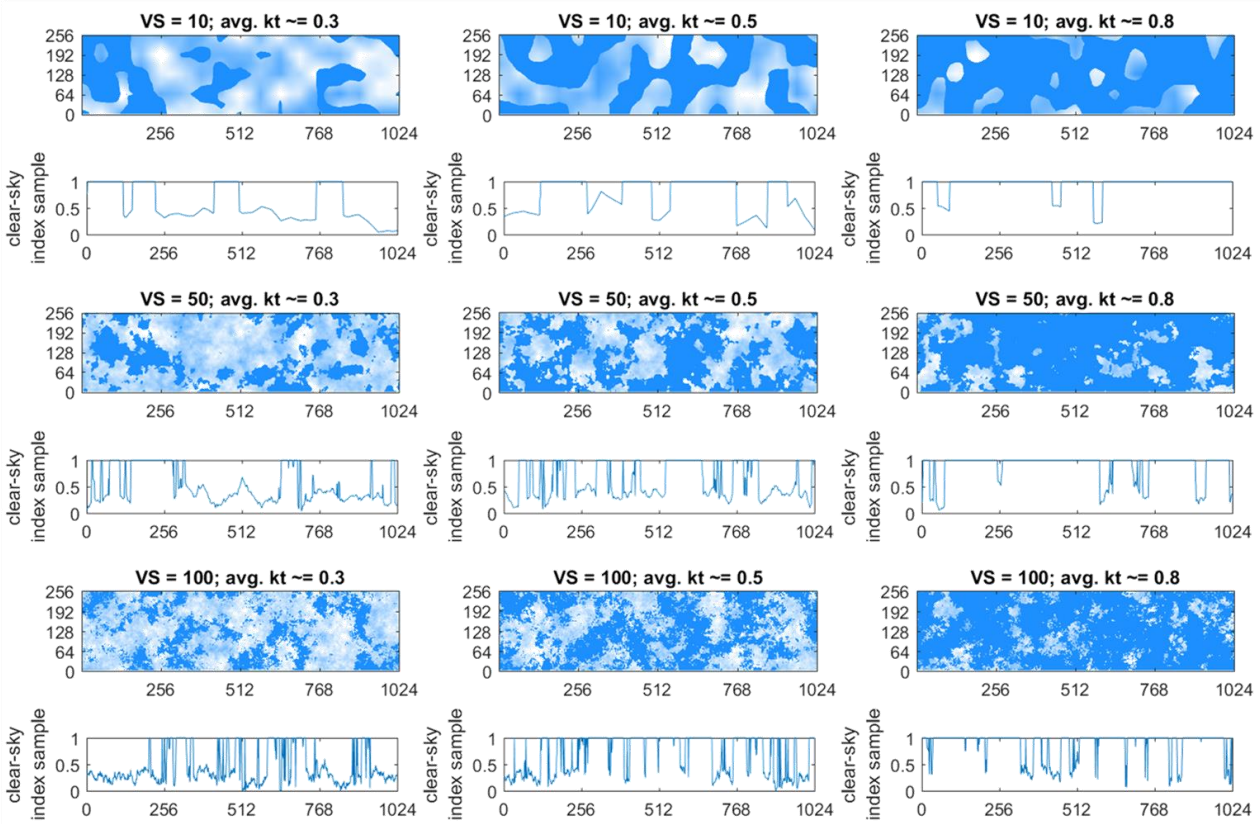

Figure 7: Cloud fields created based on each VS and kt input.

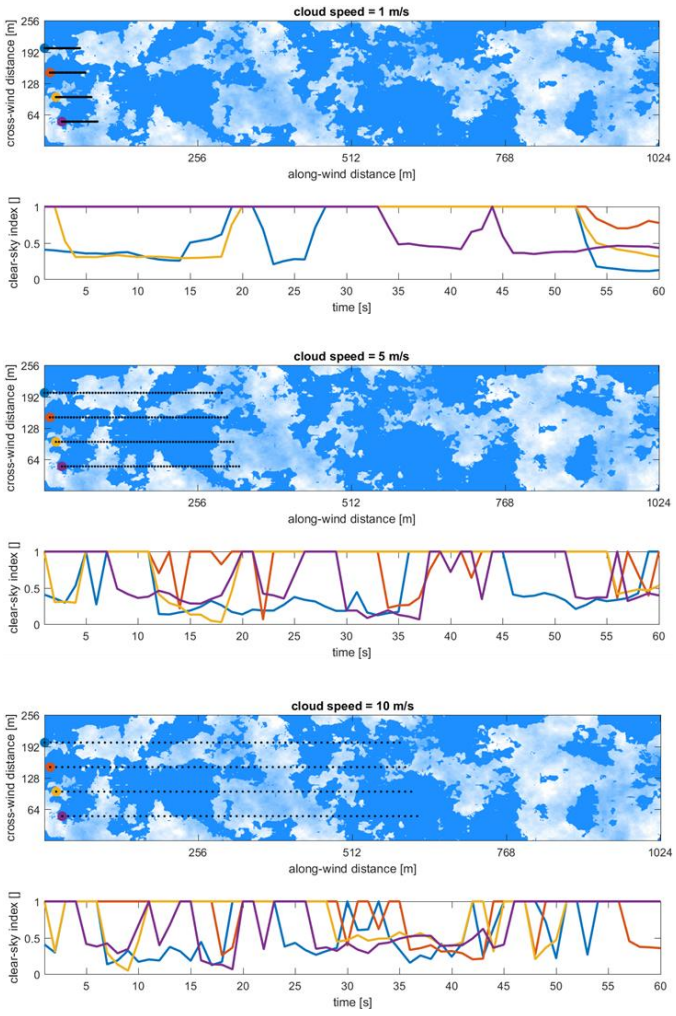

Figure 8: Timeseries created from sampling the same cloud field at different intervals corresponding to different cloud speeds.

F. Convert to GHI and Power

The samples described in Section III. E. are analogous to clear-sky index samples. They can be converted to GHI by multiplying by a clear-sky index (e.g., [10]). Figure 9 shows a sample GHI timeseries created with this method. The "on-off" behavior of the clear-sky index samples is again seen in the GHI samples.

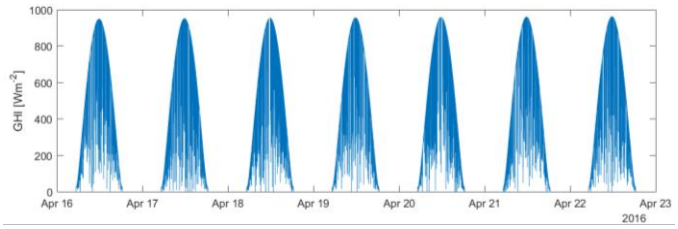

Figure 9: Sample GHI timeseries derived from cloud fields.

These GHI samples can be converted to power output samples by using a decomposition and transposition model to convert to plane of array (POA) irradiance in the plane of the PV modules to be simulated, and then by using an irradiance to power model to convert to power output.

Figure 10 shows PV power samples over a day. The VS and kt were varied over different hours of the day, so some periods are fully clear while others are cloudy. Again, we notice the "on-off" behavior of the power from the single location. However, when timeseries are sampled at hundreds of locations (corresponding to the hundreds of different transformer locations on the feeder), the aggregate output is much smoother and looks more realistic. As described in Section IV, we have ongoing tests to evaluate the need for accurate distributed PV inputs. For analysis such as voltage regulator tap changes, it may not be important that a single customer be accurately portrayed because the regulator will only see the aggregate output of several PV systems.

IV. Unique PV Profiles Impact on Distribution Studies

Previous work has shown the value of the high-frequency solar inputs discussed in Section II.B. to distribution grid studies: it was found that computing voltage regulator tap change operations using hourly PV samples instead of high-frequency samples resulted in a 20% to 70% error [2,11]. In this analysis, we additionally show the value of using unique PV inputs across the feeder (discussed in Section II.C.), instead of assuming the same PV power profile at all locations. Figure 11 shows voltage regulator timeseries for a week-long simulation for both the case of a single irradiance profile used at all PV interconnection points and for a unique irradiance profile used at each interconnection point. The unique irradiance profiles were created based on 8 ground measurements, then were spread across the feeder using the cloud speed based time

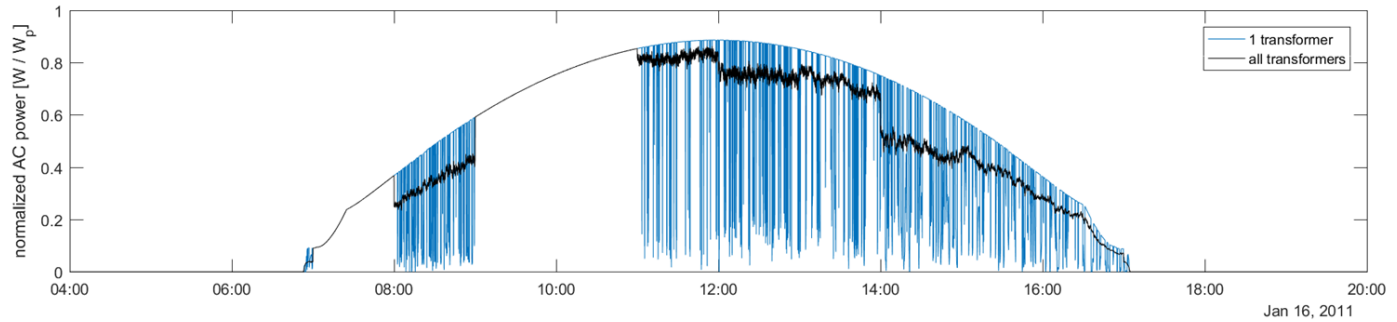

Figure 10: Sample power output timeseries for one location (blue), and for the aggregate of all locations on the feeder (black).

shifting described in section II. C.). The test feeder and shifting method are described in more detail in [12]. The result is that the unique irradiance profiles resulted in ~30% fewer tap change operations. Thus, in order to accurately determine PV impacts such as voltage regulator tap change operations, it is important to generate spatially-unique irradiance profiles.

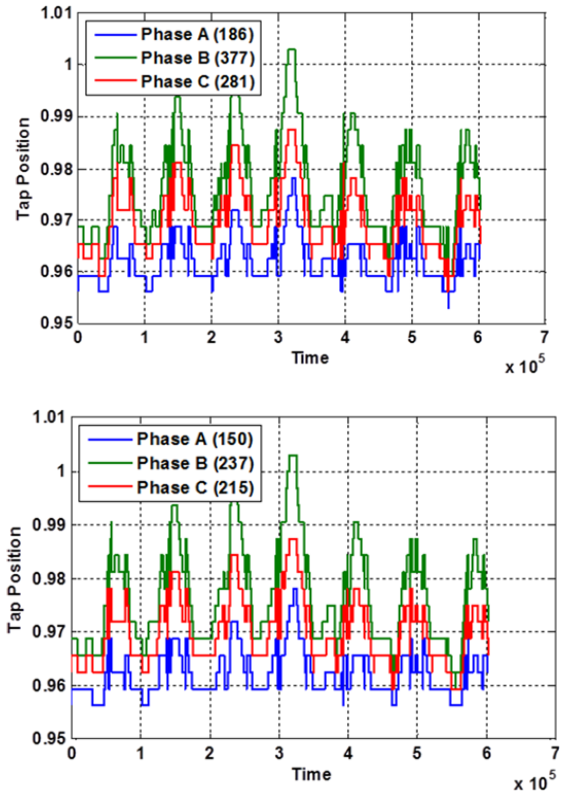

Figure 11. Voltage regulator tap change operations in a sample week for [top] a single irradiance profile used at all interconnection points and [bottom] unique irradiance profiles used at each interconnection point.

V. Conclusions and Future Work

We have shown the need for unique, high-frequency solar PV samples in quasi-static time series simulations (QSTS) of distribution grid impacts of PV, and laid out the synthetic cloud field method. Additional tweaks to the cloud field methodology are needed to make the sampled timeseries better match measured irradiance data. Additionally, the method should be further demonstrated with QSTS simulations to show its value for simulating high penetrations of distributed PV when no or limited ground data is available.

Acknowledgment

This research was supported by the DOE SunShot Initiative, under agreement 30691. Sandia National Laboratories is a multimission laboratory managed and operated by National Technology and Engineering Solutions of Sandia, LLC, a wholly owned subsidiary of Honeywell International, Inc., for the U.S. Department of Energy's National Nuclear Security Administration under contract DE-NA0003525. Report number SAND2017-5646 C.

References

[1] B. Palmintier, R. Broderick, B. Mather, et al., "On the Path to SunShot: Emerging Issues and Challenges in Integrating Solar with the Distribution System," National Renewable Energy Laboratory, NREL/TP-5D00-65331, 2016.

[2] M. J. Reno, J. Deboever, and B. Mather, "Motivation and Requirements for Quasi-Static Time Series (QSTS) for Distribution System Analysis," IEEE PES General Meeting, 2017.

[3] A. Nguyen, M. Velay, J. Schoene, V. Zheglov, B. Kurtz, K. Murray, B. Torre, and J. Kleissl, "High PV penetration impacts on five local distribution networks using high resolution solar resource assessment with sky imager and quasi-steady state distribution system simulations", *Solar Energy*, 2016.

[4] J. M. Bright, O. Babacan, J. Kleissl, P. G. Taylor, and R. Crook, "A synthetic, spatially decorrelating solar irradiance generator and application to a LV grid model with high PV penetration", *Solar Energy*, 2017.

[5] M. Lave, R. J. Broderick, and M. J. Reno, "Solar Variability Zones: Satellite-Derived Zones that Represent High-Frequency Ground Variability," *Solar Energy*, 2017.

[6] J. S. Stein, C. W. Hansen, A. Ellis, and V. Chadliev, "Estimating annual synchronized 1-min power output profiles from utility-scale PV plants at 10 locations in Nevada for a solar grid integration study," in Proceedings of the 26th European Photovoltaic Solar Energy Conference and Exhibition, 2011.

[7] K. Perlin, "Implementing improved perlin noise," GPU Gems, pp. 73-85, 2004.

[8] .Lave, M. J. Reno, and R. J. Broderick, "Characterizing Local High-Frequency Solar Variability and its Impact to Distribution Studies," *Solar Energy*, 2015.

[9] M. J. Reno and J. S. Stein, "Using Cloud Classification to Model Solar Variability," in ASES National Solar Conference, Baltimore, MD, 2013.

[10] M. Lave, J. S. Stein, and A. Ellis. "Analyzing and simulating the reduction in PV powerplant variability due to geographic smoothing in Ota City, Japan and Alamosa, CO." IEEE Photovoltaic Specialists Conference (PVSC), 2012.

[11] M. Lave, J. Quiroz, M. Reno, and R. Broderick, "High Temporal Resolution Load Variability Compared to PV Variability," IEEE Photovoltaic Specialists Conference (PVSC), 2016.

[12] M. J. Reno, M. Lave, J. E. Quiroz, and R. J. Broderick, "PV Ramp Rate Smoothing Using Energy Storage to Mitigate Increased Voltage Regulator Tapping," IEEE Photovoltaic Specialists Conference (PVSC), 2016.

.